Constraining η/s through high-$p_\perp$ theory and data

Bithika Karmakar, Dusan Zigic, Igor Salom, and Magdalena Djordjevic[*]
Institute of Physics Belgrade, University of Belgrade, Belgrade 11080, Serbia

Jussi Auvinen
Institute of Physics Belgrade, University of Belgrade, Belgrade 11080, Serbia
and University of Jyväskylä, Jyväskylä P.O. Box 35, FI-40014, Finland

Pasi Huovinen
Incubator of Scientific Excellence—Centre for Simulations of Superdense Fluids, University of Wrocław, Wrocław 50-204, Poland

Marko Djordjevic
Faculty of Biology, University of Belgrade, Belgrade 11000, Serbia

We study whether it is possible to use high-$p_\perp$ data/theory to constrain the temperature dependence of the shear viscosity over entropy density ratio η/s of the matter formed in ultrarelativistic heavy-ion collisions at the BNL Relativistic Heavy Ion Collider (RHIC) and the CERN Large Hadron Collider (LHC). We use two approaches: (i) We calculate high-$p_\perp$ R_{AA} and flow coefficients v_2, v_3, and v_4 assuming different $(\eta/s)(T)$ of the fluid-dynamically evolving medium. (ii) We calculate the quenching strength $(\hat{q}/T^3)$ from our dynamical energy loss model and convert it to η/s as a function of temperature. It turned out that the first approach cannot distinguish between different $(\eta/s)(T)$ assumptions when the evolution is constrained to reproduce the low-$p_\perp$ data. In distinction, $(\eta/s)(T)$ calculated using the second approach agrees surprisingly well with the $(\eta/s)(T)$ inferred through state-of-the-art Bayesian analyses of the low-$p_\perp$ data even in the vicinity of T_c, while providing much smaller uncertainties at high temperatures.

I. INTRODUCTION

Quantum chromodynamics (QCD) predicts that at extremely high densities matter undergoes a transition to a state consisting of deconfined and interacting quarks, antiquarks, and gluons [1,2]. According to the current cosmology, this new state of matter, called quark-gluon plasma (QGP) [3], existed immediately after the big bang [4]. Today, QGP is created in "little bangs," when heavy ions collide at ultrarelativistic energies [5] in experiments at the BNL Relativistic Heavy Ion Collider (RHIC) and the CERN Large Hadron Collider (LHC). Such collisions lead to an expanding fireball of quarks and gluons, which thermalizes to form QGP. The QGP cools down, and quarks and gluons hadronize when the temperature T drops to the critical temperature T_c.

*Email: magda@ipb.ac.rs

Extracting useful information from "little bangs" requires comparing theoretical predictions with experimental data. By such comparisons, it is established that QGP is formed in the RHIC and LHC experiments [6] through two main lines of evidence [5–7]: (i) by comparison of low transverse momentum ($p_\perp$) measurements with relativistic hydrodynamical predictions, which imply that created QGP is consistent with the description of a nearly perfect fluid [8–10], and (ii) by comparison of perturbative QCD (pQCD) predictions with high-$p_\perp$ data [11–14], which showed that high-$p_\perp$ partons (jets) significantly interact with the opaque medium [5]. Beyond the discovery phase, the current challenge is to investigate the properties of this extreme form of matter [15–25].

The QGP was expected to behave as a weakly interacting gas based on ideas of asymptotic freedom and color screening [26]. Thus, the agreement of the fluid-dynamical predictions, which assumed the QGP to behave as a nearly inviscid fluid, with the data came as a surprise [10]. Furthermore, subsequent calculations revealed [10] that reproduction of the data required the shear viscosity to entropy density ratio (η/s) of QGP to be near the lower bound predicted by anti–de Sitter and conformal field theory (AdS/CFT) correspondence [27].

However, the temperature of the QGP changes significantly [28] during the evolution of the collision system. For example, in the LHC experiments, the temperature is estimated

to span the range from $4T_c$ to T_c. Even if the QGP behaves as a perfect fluid close to T_c (the "soft," strongly coupled regime), its η/s may significantly increase with increasing T if the QGP becomes weakly coupled at higher temperatures (the "hard," weakly coupled regime). We call this possibility the "soft-to-hard" medium hypothesis.

Testing this hypothesis has turned out to be surprisingly difficult. Reproduction of the observed anisotropies of low-$p_\perp$ particles necessitates low η/s in the vicinity of T_c, but the value of shear viscosity in higher temperatures has only a weak effect on anisotropies in collisions at LHC energies, and basically no effect at all at RHIC [29–31]. In the recent Bayesian analyses of the data, this is manifested in a well constrained η/s in the $T_c \lesssim T \lesssim 1.5 T_c$ temperature range and weak constraints at larger temperatures [17–20]. Some of the most recent Bayesian analyses [32,33] even suggest that η/s may decrease in the region T_c–$2T_c$, where the reason for such a decrease still remains to be understood.

Thus, it is evident that a complementary theory and observables are needed to investigate the "soft-to-hard" medium hypothesis. Since most of the jet energy loss takes place when the system is hottest, it is reasonable to expect the high-$p_\perp$ observables to be sensitive to the properties of the system at that stage. To use jet energy loss and high-$p_\perp$ data to provide constraints to the bulk properties of the collision system, we developed the state-of-the-art DREENA tomography tool [34,35] based on the dynamical energy loss formalism [36–38]. So far, we have used this tool to, e.g., provide constraints to the early evolution of the collision system [22] and map how the shape of the collision system is manifested in the high-$p_\perp$ data [23].

In this study, we explore whether high-$p_\perp$ data can provide constraints on the η/s ratio of QGP at high temperatures. As is known, shear viscosity generates entropy, which means that the system with larger viscosity cools slower or, alternatively, to reach the same final entropy, the system with larger viscosity must have a lower initial temperature. Thus, different assumed η/s during the early evolution of the system may lead to different jet energy loss and therefore different nuclear suppression factor R_{AA}. As well, azimuthal anisotropy in path lengths and temperature along the paths leads to azimuthal dependence of jet suppression [5], which is measured as v_n of high-$p_\perp$ particles. High-$p_\perp$ v_n are known to be sensitive to the details of the medium evolution [34,35,39], and, since viscosity changes the evolution of the anisotropy of the system, the changes in η/s can lead to changes in high-$p_\perp$ v_n. We choose three different parametrizations of $(\eta/s)(T)$, adjust the parameters to reproduce the low-$p_\perp$ data measured in $\sqrt{s_{NN}} = 200$ GeV Au + Au collisions (RHIC) and $\sqrt{s_{NN}} = 5.02$ TeV Pb + Pb collisions (LHC), calculate the temperature evolution of the system, and energy loss of jets traversing this system in each case, and evaluate the R_{AA} and high-$p_\perp$ v_2, v_3, and v_4 to see if different assumptions of η/s lead to differences in these observables.

Complementary to this phenomenological approach to infer the η/s ratio from the experimental data, we also provide a fully theoretical estimate of η/s based on jet energy loss: The jet quenching strength is quantified through the jet quenching parameter $\hat{q}$. It has been argued that in a weakly coupled

regime $T^3/\hat{q}$ is directly proportional to η/s [40], and thus evaluating one allows one to know the other. We estimate the quenching parameter $\hat{q}$ as function of temperature using our dynamical energy loss formalism, convert it to η/s, and compare the resulting $(\eta/s)(T)$ to constraints obtained from state-of-the-art Bayesian analyses [18,19].

II. METHODS

A. Modeling the bulk evolution

To calculate the temperature evolution and the low-$p_\perp$ observables we use the version of VISHNEW [41,42] used in Refs. [17,18,43].[1] It is a code to solve the dissipative fluid-dynamical equations in 2+1 dimensions, i.e., assuming boost invariance. Shear stress and bulk pressure are taken as dynamical variables and evolved according to the Israel-Stewart type equations [45]. We use an equation of state (EoS) [43] that combines the lattice QCD-based EoS of the HotQCD Collaboration [46] at large temperatures and a hadron resonance gas EoS at low temperatures. At a constant temperature $T_{\rm sw} = 151$ MeV hypersurface, we convert the fluid to particle ensembles according to the Cooper-Frye prescription [47]. These ensembles are fed to the UrQMD hadron cascade [48,49], which describes the evolution of the hadronic stage of the system until freeze-out.

We generate the event-by-event fluctuating initial states using the T$_R$ENTo model [50]. In this model nucleus-nucleus collisions are considered as a superposition of nucleon-nucleon collisions. The nucleons are represented by Gaussian distributions, which in this study have the width $w = 0.5$ fm while the minimum nucleon-nucleon distance within the nucleus is also set to $d = 0.5$ fm. The inelastic nucleon-nucleon cross section is 70 mb at $\sqrt{s_{\rm NN}} = 5.02$ TeV (energy of Pb + Pb collisions) and 42 mb at $\sqrt{s_{\rm NN}} = 200$ GeV (energy of Au + Au collisions). For the other parameters we use the maximum *a posteriori* (MAP) values found in Ref. [18]. We do not allow any preequilibrium evolution (free-streaming or otherwise), and use $\tau_0 = 1$ fm/c as the initial time for fluid-dynamical evolution, since the reproduction of the high-$p_\perp$ observables does not allow strong transverse expansion earlier [22].

We include both bulk and shear viscosity in our fluid-dynamical calculation. The temperature dependence of the bulk viscosity coefficient ζ is parametrized as a Cauchy distribution [18]:

$$(\zeta/s)(T) = \frac{(\zeta/s)_{\rm max}}{1 + \left(\frac{T - T_0}{(\zeta/s)_{\rm width}}\right)^2}. \quad (1)$$

We consider a small bulk viscosity with a maximum value $(\zeta/s)_{\rm max} = 0.03$, the width parameter $(\zeta/s)_{\rm width} = 0.022$, and $T_0 = 0.183$ GeV. As in the case of the T$_R$ENTo parameters described above, the width and T_0 correspond to MAP parameter values from Ref. [18]. However, the maximum of the bulk viscosity [$(\zeta/s)_{\rm max}$] is decreased compared to the MAP

---

[1]Code available at [44].

value in [18] to compensate for the lack of preequilibrium free streaming and still reach agreement with the $p_\perp$ spectra.

As mentioned, our main objective is to find out whether high-$p_\perp$ data can provide constraints to η/s at high temperatures. Naively one can expect the jet energy loss to be proportional to the third power of temperature (T^3), but a detailed calculation has shown it to be proportional to only

$T^{1.2}$ [51,52]. Since the sensitivity to temperature is weaker than expected, we want to maximize the difference in temperature due to differences in η/s. Therefore we do not take as our $(\eta/s)(T)$ the upper and lower limits suggested by the Bayesian analyses [18,19] but something more extreme. We parametrize the temperature dependence of η/s as [17,18]

$$(\eta/s)(T) = \begin{cases} (\eta/s)_{\min}, & T < T_c, \\ (\eta/s)_{\min} + (\eta/s)_{\text{slope}}(T - T_c)\left(\frac{T}{T_c}\right)^{(\eta/s)_{\text{crv}}}, & T > T_c, \end{cases} \tag{2}$$

where $(\eta/s)_{\min}$ is the minimum value of the specific shear viscosity, $(\eta/s)_{\text{slope}}$ is the slope above T_c, and $(\eta/s)_{\text{crv}}$ controls the curvature above T_c. T_c is fixed to the pseudo-critical temperature $T_c = 154$ MeV evaluated by the HotQCD Collaboration [46].

We study three different scenarios, each capable of describing a subset of low-$p_\perp$ data at RHIC and LHC with reasonable accuracy:

(1) constant η/s (0.15 for Pb + Pb collision at LHC and 0.12 for Au + Au collision at RHIC),
(2) $(\eta/s)_{\min} = 0.1$, $(\eta/s)_{\text{slope}} = 1.11$, $(\eta/s)_{\text{crv}} = -0.48$,
(3) $(\eta/s)_{\min} = 0.04$, $(\eta/s)_{\text{slope}} = 3.30$, $(\eta/s)_{\text{crv}} = 0$.

The parameters in our second scenario are within the 90% credible intervals of the analysis of Ref. [18]. Therefore, we label it as "Nature." Nevertheless, our $(\eta/s)_{\min}$ is larger than in Ref. [18] since we require the reproduction of the RHIC data, not only the LHC data. As is known, including the RHIC data tends to increase the favored minimum value of η/s [20]. Our third scenario with its very rapidly rising η/s (see Fig. 8) is inspired by the "LHHQ" parametrization in Ref. [30]. Consequently, we label it as such.

To calculate the low-$p_\perp$ and high-$p_\perp$ predictions, we generated 10^4 minimum-bias events and sorted the events in centrality classes according to the number of participants. While using the final particle multiplicity would be closer to the centrality selection done in experiments, participant number sorting allows us to reduce the number of hydrodynamic simulations by focusing on the narrower (10–50)% centrality range, thus saving computational resources (we numerically tested that this approximation would have a negligible effect on theoretical predictions). Finally, we evaluated the event-averaged observables in each centrality bin.

We reproduced the pion, kaon, and proton multiplicities and charged hadron four-particle cumulant elliptic flow $v_2\{4\}$ in Au + Au collisions at $\sqrt{s_{NN}} = 200$ GeV (RHIC) and Pb + Pb collisions at $\sqrt{s_{NN}} = 5.02$ TeV (LHC) in 10–20%, 20–30%, 30–40%, and 40–50% centrality classes by varying only the nucleon-nucleon cross section according to the collision energy and the overall normalization factor according to the collision energy and choice of $(\eta/s)(T)$. All the other T$_R$ENTo parameters were kept the same in all cases. For the LHHQ parametrization, the minimum value of η/s is chosen to get an acceptable agreement of $v_2\{4\}$ with both Pb + Pb and Au + Au collision data. The centrality dependence of charged

particle multiplicities ($p_\perp$-integrated yields) for Pb + Pb and Au + Au collisions with three different $(\eta/s)(T)$ parametrizations found from the hydrodynamical simulation are shown in the left panels of Fig. 1. The four-particle elliptic flow coefficient $v_2\{4\}$ at different centrality classes for Pb + Pb and Au + Au collisions are shown in the right panels of Fig. 1.

B. Overview of DREENA framework

After evaluating the temperature evolution, we use the "generalized DREENA-A" framework to calculate the high-$p_\perp$ observables: Nuclear suppression factor R_{AA} and high-$p_\perp$ flow harmonics v_2, v_3, and v_4. DREENA (Dynamical Radiative and Elastic ENergy loss Approach) is a computationally efficient tool for QGP tomography [34,35], based on generalized hard thermal loop (HTL) perturbation theory [57] with naturally regulated infrared divergences [36,58]. In this formalism both the radiative [37,38] and collisional energy loss [36] of high energy particles have been computed in an evolving QCD medium of finite size at finite temperature. Furthermore, the framework is extended to account for running coupling [59], finite magnetic mass [60], and beyond soft-gluon approximation [58]. We also recently extended the formalism towards finite orders in opacity [61], but showed that higher-order effects can be neglected for high-$p_\perp$ predictions. Thus, a computationally more efficient version with one scattering center is used in this study. Additionally, in this framework, all parameters are fixed to standard literature values stated below (i.e., no fitting parameters are used) [22,23]. This allows systematic comparison of data and the predictions from the simulation obtained using the same formalism and parameter set.

We use the generic pQCD convolution formula [59,62] to generate the final quenched (q) and unquenched (u) spectra of hadrons as

$$\frac{E_f d^3\sigma_q(H_Q)}{dp_f^3} = \frac{E_i d^3\sigma(Q)}{dp_i^3} \otimes P(E_i \rightarrow E_f) \otimes D(Q \rightarrow H_Q), \tag{3}$$

$$\frac{E_f d^3\sigma_u(H_Q)}{dp_f^3} = \frac{E_i d^3\sigma(Q)}{dp_i^3} \otimes D(Q \rightarrow H_Q), \tag{4}$$

where i and f denote the initial parton (Q) and the final hadron (H_Q) respectively. $\frac{E_i d^3\sigma(Q)}{dp_i^3}$ represents the initial parton spectrum calculated at the next-to-leading order for light
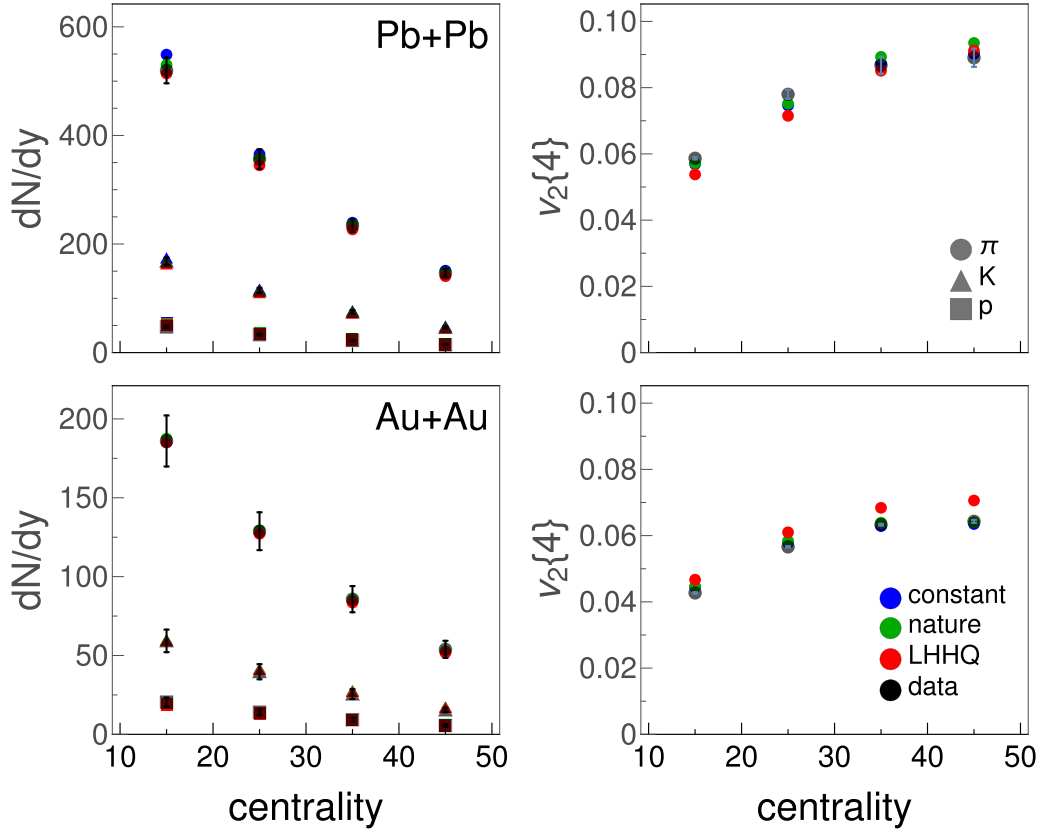
FIG. 1. Left panels: Centrality dependence of the $p_\perp$-integrated yields of pions, kaons, and protons are shown in different centrality classes. The pion multiplicity is scaled by 0.5. The upper panel corresponds to 5.02 TeV Pb + Pb collisions, where the ALICE experimental data are taken from Ref. [53]. The lower panel corresponds to 200 GeV Au + Au collisions, where the PHENIX experimental data are taken from Ref. [54]. Right panels: $v_2\{4\}$ is shown at different centrality classes. The upper panel corresponds to 5.02 TeV Pb + Pb collisions, where the ALICE experimental data are taken from Ref. [55]. The lower panel corresponds to 200 GeV Au + Au collisions, where the STAR experimental data are taken from Ref. [56].

and heavy partons [63–65]. $P(E_i \rightarrow E_f)$ is the energy loss probability computed within finite temperature field theory. $D(Q \rightarrow H_Q)$ represents the fragmentation function. DSS [66], BCFY [67,68], and KLP [69] fragmentation functions were used for charged hadrons, D mesons, and B mesons, respectively. DREENA-A [35], where "A" stands for adaptive (i.e., arbitrary) temperature profiles, has been optimized to incorporate any event-by-event fluctuating temperature profile [34]. For parameters, we use $\Lambda_{\mathrm{QCD}} = 0.2$ GeV [70–72] and the effective numbers of light quark flavors, $n_f = 3$ and 2.5 for Pb + Pb and Au + Au collision systems, respectively. We also consider the gluon mass $m_g = \mu_E/\sqrt{2}$ [73], where μ_E is the temperature-dependent Debye mass computed following the procedure in Ref. [70] (outlined in the next subsection). We assume the mass of the light quarks to be $\mu_E/6$, and the masses of the charm and bottom quarks to be 1.2 and 4.75 GeV, respectively. The magnetic-to-electric mass ratio is $\mu_M/\mu_E = 0.6$ [74].

C. Derivation of transport coefficient $\hat{q}$ from dynamical energy loss formalism

To derive the transport coefficient $\hat{q}$, which is the squared average transverse momentum exchange between the medium

and the fast parton per unit path length [75], we start from dynamical *perturbative* QCD medium, where the interaction between high-$p_\perp$ partons and QGP constituents can be characterized by the HTL resummed elastic collision rate [76]:

$$\frac{d\Gamma_{el}}{d^2q} = 4C_A\left(1 + \frac{n_f}{6}\right)T^3 \frac{\alpha_s^2}{q^2(q^2 + \mu_E^2)}. \quad (5)$$

While α_s in Eq. (5) is presumed to be constant, for RHIC and LHC, it is necessary to include running coupling constant in the kernel due to the wide kinematic range covered in these experiments. To include running coupling in dynamical energy loss formalism, we adopt the procedure from Ref. [77] where

$$\alpha_s^2 \rightarrow \alpha_s(ET)\alpha_s(\mu_E^2), \quad (6)$$

and μ_E is obtained [70] as a self-consistent solution to

$$\mu_E^2 = \left(1 + \frac{n_f}{6}\right)4\pi\alpha(\mu_E^2)T^2, \quad (7)$$

where

$$\alpha(t) = \frac{4\pi}{(11 - \frac{2}{3}n_f)} \frac{1}{\ln\left(\frac{t}{\Lambda^2}\right)}, \quad (8)$$

leading to

$$\mu_E = \sqrt{\Lambda^2 \frac{\xi(T)}{W(\xi(T))}}, \qquad (9)$$

where

$$\xi(T) = \frac{1 + \frac{n_f}{6}}{11 - \frac{2}{3}n_f}\left(\frac{4\pi T}{\Lambda}\right)^2, \qquad (10)$$

and W is Lambert's W function. Note that μ_E obtained through this procedure agrees with lattice QCD results [70].

By using Eqs. (9) and (6), Eq. (5) reduces to

$$\frac{d\Gamma_{el}}{d^2q} = \frac{C_A}{\pi}T\frac{\alpha(ET)\mu_E^2}{q^2(q^2 + \mu_E^2)}, \qquad (11)$$

which reproduces Eq. (16) from Ref. [76] in the case of constant coupling $\alpha(ET) = g^2/4\pi$. Following Ref. [60], finite magnetic mass can be introduced into Eq. (11), reducing the collision rate to

$$\frac{d^2\Gamma_{el}}{d^2q} = \frac{C_A}{\pi}T\alpha(ET)\frac{\mu_E^2 - \mu_M^2}{(q^2 + \mu_E^2)(q^2 + \mu_M^2)}, \qquad (12)$$

where μ_M is the magnetic mass defined in the previous subsection, and $C_A = 4/3$. This expression [i.e., Eq. (12)] can be further reduced to

$$\frac{d\Gamma_{el}}{d^2q} = \frac{C_A}{\pi}T\alpha(ET)\left(\frac{1}{q^2 + \mu_M^2} - \frac{1}{q^2 + \mu_E^2}\right). \qquad (13)$$

In the fluid rest frame, the transport coefficient $\hat{q}$ can then be computed as [76,78]

$$
\begin{aligned}
\hat{q} &= \int_0^{\sqrt{6ET}} d^2q\, q^2 \frac{d\Gamma_{el}}{d^2q} \\
&= C_A T\alpha(ET)\int_0^{6ET} dq^2\, q^2\left(\frac{1}{q^2 + \mu_M^2} - \frac{1}{q^2 + \mu_E^2}\right) \\
&= C_A T \frac{4\pi}{(11 - \frac{2}{3}n_f)} \frac{\left(\mu_E^2 \ln\left[\frac{6ET + \mu_E^2}{\mu E^2}\right] - \mu_M^2 \ln\left[\frac{6ET + \mu_M^2}{\mu_M^2}\right]\right)}{\ln\left(\frac{ET}{\Lambda^2}\right)}.
\end{aligned}
\qquad (14)
$$

In the limit $ET \to \infty$, Eq. (14) reduces to an expression independent of jet E:

$$
\begin{aligned}
\hat{q} &= C_A T \frac{4\pi}{11 - \frac{2}{3}n_F}\left(\mu_E^2 \frac{\ln\frac{ET}{\mu_E^2/6}}{\ln\frac{ET}{\Lambda^2}} - \mu_M^2 \frac{\ln\frac{ET}{\mu_M^2/6}}{\ln\frac{ET}{\Lambda^2}}\right) \\
&\approx C_A T \frac{4\pi}{11 - \frac{2}{3}n_F}\left(\mu_E^2 - \mu_M^2\right) \\
&= C_A T \frac{4\pi}{11 - \frac{2}{3}n_F}\frac{1 + \frac{n_F}{6}}{11 - \frac{2}{3}n_F}\frac{(4\pi)^2 T^2}{W(\xi(T))}\left(1 - x_{ME}^2\right) \\
&= C_A \left(\frac{4\pi}{11 - \frac{2}{3}n_F}\right)^2 \frac{4\pi\left(1 + \frac{n_F}{6}\right)}{W(\xi(T))}\left(1 - x_{ME}^2\right)T^3, \qquad (15)
\end{aligned}
$$

where $x_{ME} = \mu_M/\mu_E$ is the magnetic-to-electric mass ratio. It is worth noticing that this is expected behavior: As a property of the medium, $\hat{q}$ should be independent (or weakly dependent) on jet energy [76]. Nevertheless, many models/approaches fail to describe this behavior [76].

III. RESULTS

A. Constraining η/s through high-$p_\perp$ data

To examine the sensitivity of the high-$p_\perp$ observables on the specific shear viscosity of the medium, we compare in Fig. 2 the experimental charged hadron R_{AA} and high-$p_\perp$ flow harmonics v_2, v_3, and v_4 in Pb + Pb collisions at $\sqrt{s_{NN}} = 5.02$ TeV to the theoretical predictions calculated using three different $(\eta/s)(T)$ parametrizations (see Sec. II A). The high-$p_\perp$ flow harmonics are computed using the scalar product method [34]. As seen in all three cases, the calculated charged hadron R_{AA} and flow anisotropies are almost indistinguishable from each other. Furthermore, the predicted charged hadron v_4 significantly underestimates the experimental data even when the current large experimental uncertainties are taken into account. We previously reported a similar observation in Ref. [34], where high-$p_\perp$ v_4 was calculated using several different initializations of the fluid dynamical evolution.

Unfortunately, the heavy flavor high-$p_\perp$ observables shown in Fig. 3 are hardly more sensitive to the $(\eta/s)(T)$ parametrizations. The calculated D and B meson R_{AA}, v_2, and v_3 in Pb + Pb collisions at $\sqrt{s_{NN}} = 5.02$ TeV do not depend on our assumptions about η/s, whereas v_4 in the 10–30% centrality class shows some sensitivity. Nevertheless, given the large experimental uncertainties of v_2 and v_3, it is doubtful whether the small difference in v_4 is experimentally detectable, especially when our v_4 predictions are very close to 0.

Since the collisions at LHC reach larger initial temperatures than collisions at RHIC, we may expect them to be more sensitive to η/s at large temperatures, and thus to our $(\eta/s)(T)$ parametrizations. Nevertheless, for the sake of completeness and to allow for surprises in the evolution, we checked whether the high-$p_\perp$ observables measured in collisions at the full RHIC energy ($\sqrt{s_{NN}} = 200$ GeV) allow us to distinguish between different $(\eta/s)(T)$ parametrizations.

The theoretical predictions for charged hadron and D and B meson high-$p_\perp$ observables in Au + Au collisions at $\sqrt{s_{NN}} = 200$ GeV collision energy are shown in Figs. 4 and 5, respectively. Again, we calculated our predictions using the generalized DREENA-A framework with three different $(\eta/s)(T)$ parametrizations. As can be seen, the high-$p_\perp$ observables are not sensitive to the η/s ratio at high temperatures, and thus we cannot further constrain $(\eta/s)(T)$ using high-$p_\perp$ observables.

As was argued in the Introduction, different η/s require different initial temperatures. However, as shown in Fig. 6, temperature difference during the evolution is small and, as demonstrated above, insufficient to lead to observable differences in high-$p_\perp$ observables. In Fig. 6, we characterize the system temperature using the so-called average jet-perceived temperature: At each time τ we average the system temperature in the transverse plane using the number of jets at each point as weight; e.g., while the average initial temperature in (10–20)% centrality class for Pb + Pb collisions at
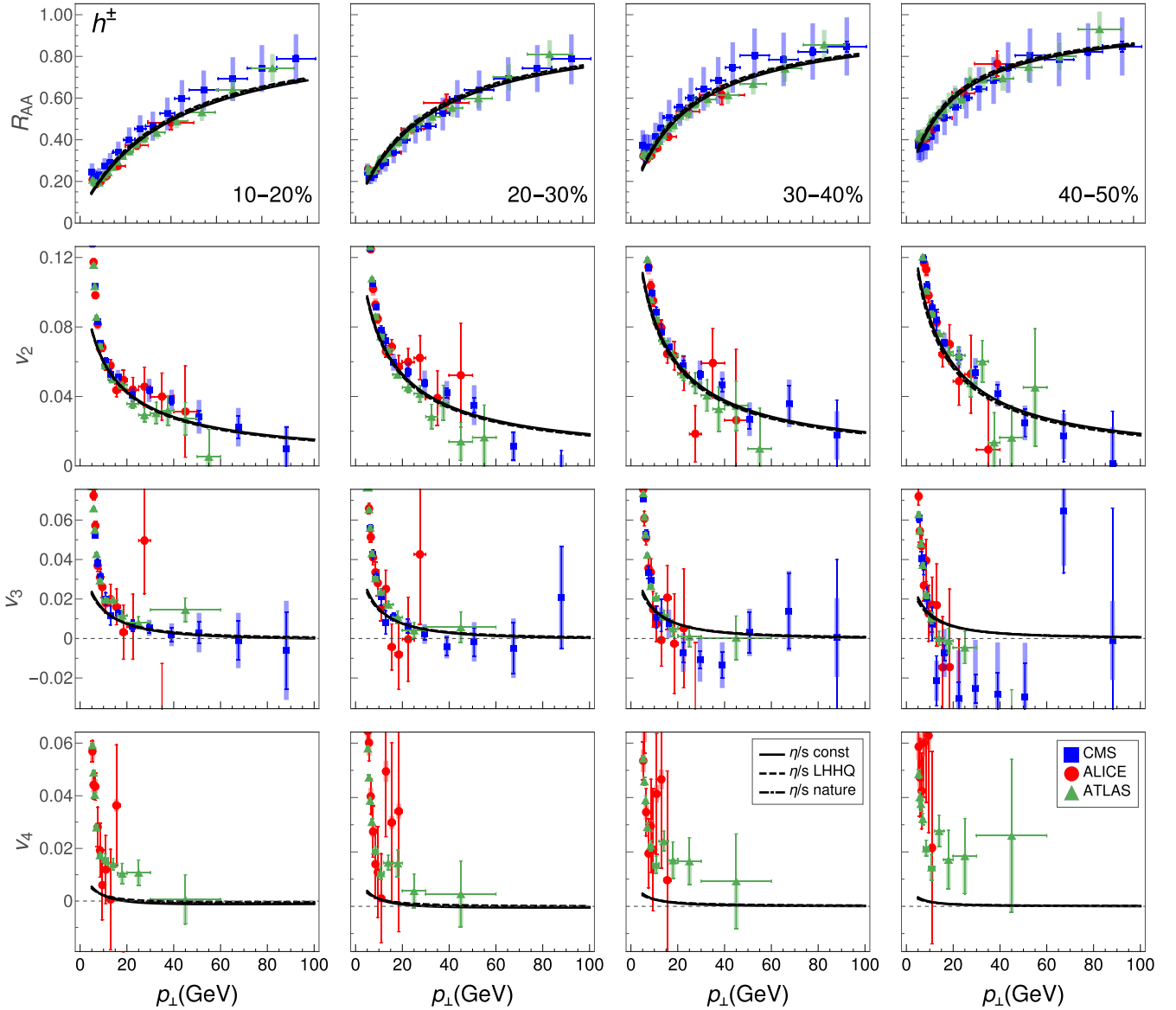
FIG. 2. Charged hadron R_{AA} (first row) and high-$p_\perp$ flow harmonics v_2 (second row), v_3 (third row), and v_4 (fourth row) as a function of transverse momentum in Pb + Pb collisions at $\sqrt{s_{NN}} = 5.02$ TeV for different $(\eta/s)(T)$ parametrizations indicated in the legend. CMS (blue squares) [79,80], ALICE (red circles) [81,82], and ATLAS (green triangles) [83,84] experimental data are also shown for comparison. Columns 1–4 represent the centrality classes 10–20%, 20–30%, 30–40%, and 40–50%, respectively.

$\sqrt{s} = 5.02$ TeV is 370 MeV, the maximal temperature experienced by the jet can reach up to 600 MeV. The jet-perceived temperatures calculated using all three $(\eta/s)(T)$ parametrizations are almost identical, differing less than 4% at the early stages of the evolution and settling for less than 2% for most of the evolution. The differences in the anisotropy of the jet-perceived temperature, $\langle jT_2 \rangle$, introduced in Ref. [23], are equally small (not shown). The investigated high-$p_\perp$ observables turned out to be insensitive to such small differences in temperature.

Even if our calculated high-$p_\perp$ R_{AA} and v_2 agree with the data (see Fig. 2), the calculated $\langle jT_2 \rangle$ are slightly below the experimentally favored values. This deviation is possible since our results for both R_{AA} and v_2 are at the lower end of experimental uncertainty. When taking the ratio

$v_2/(1 - R_{AA})$, which constrains $\langle jT_2 \rangle$, this deviation from the data is magnified, and the calculated $\langle jT_2 \rangle$ is below the experimental constraint. Nevertheless the values of $\langle jT_2 \rangle$ obtained in these calculations are close to the largest values obtained in Ref. [23] for various initialization models.

B. Calculating η/s from the dynamical energy loss $\hat{q}$

In our previous publications, we have seen that the DREENA framework is capable of reproducing the observed R_{AA} without fitting parameters [59,93,94] (see also comparison to R_{AA} in the previous subsection). This agreement suggests that the dynamical energy loss formalism can adequately describe interactions between high-$p_\perp$ particles and the QCD medium. Thus, it seems reasonable to estimate $(\eta/s)(T)$ theoretically using the dynamical energy loss model.
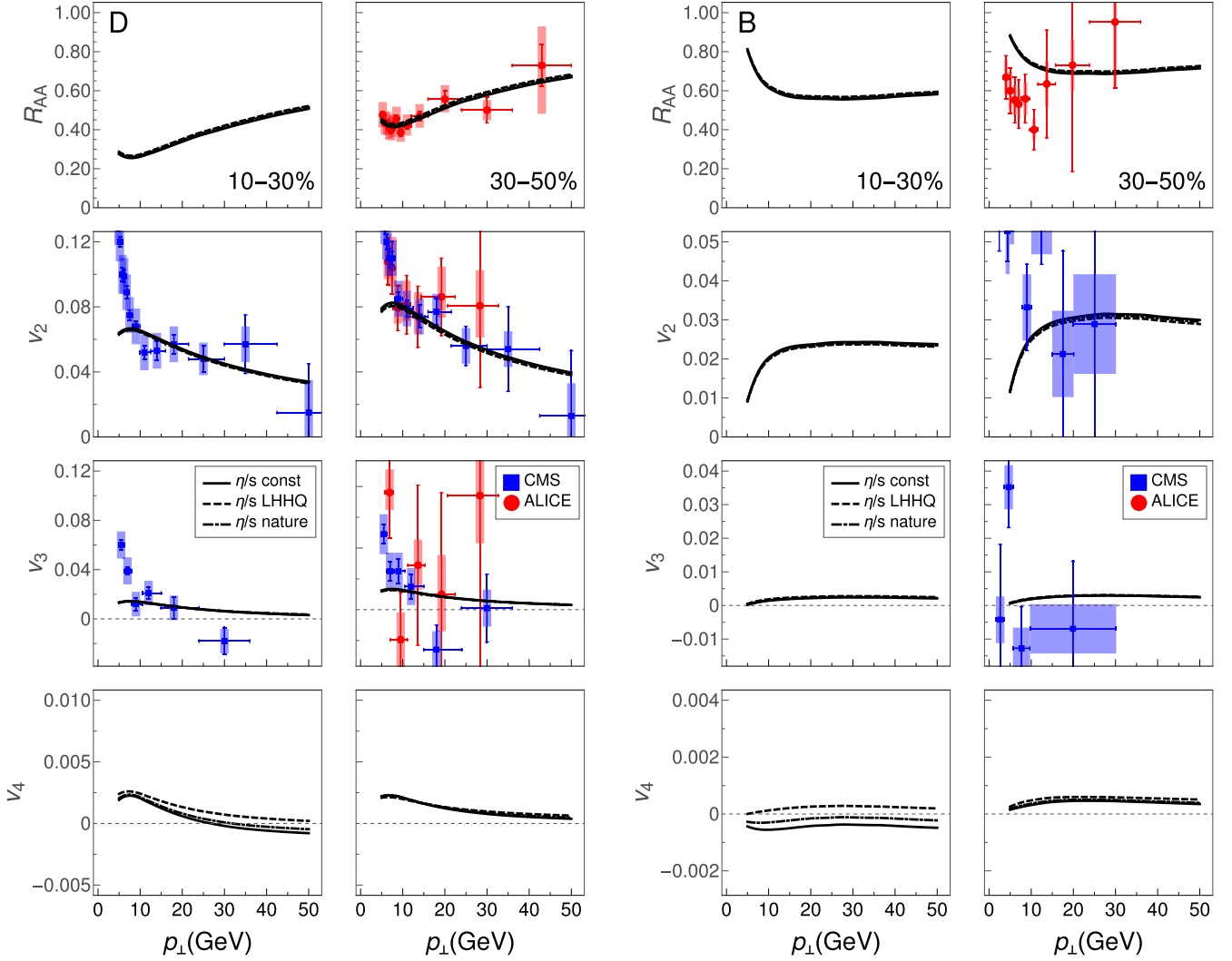
FIG. 3. Predictions for D (left 4×2 panel) and B meson (right 4×2 panel) R_{AA} (first row) and high-$p_\perp$ flow harmonics v_2 (second row), v_3 (third row), and v_4 (fourth row) using three different $(\eta/s)(T)$ parametrizations at various centralities in Pb + Pb collisions at $\sqrt{s_{NN}} = 5.02$ TeV. The theoretical predictions for D mesons are compared with the CMS (blue squares) [85] and ALICE (red circles) [86,87] data, whereas B meson predictions are compared to preliminary CMS (blue squares) [88] and preliminary ALICE (red circles) [89] data.

For this purpose, we need to estimate the jet quenching parameter $\hat{q}$, quantifying the transverse momentum broadening of fast parton due to its elastic scatterings with the medium [75]. This parameter is a key quantity in estimating the interaction strength between jet partons and nuclear matter [76,97–101]. It has been proposed to be a valuable tool for various purposes, including gaining insights into the jet quenching phenomenon, estimating the bulk medium property $(\eta/s)(T)$ [40,102], and, more recently, exploring the QCD phase diagram [103].

We presented the derivation of the transport coefficient $\hat{q}$ from our dynamical energy loss model in Sec. II C. We note that $\hat{q}$ is weakly dependent on E due to $\ln(ET)$ appearing both in the numerator and the denominator of Eq. (14), as desired for a medium property such as transport coefficient.

Before discussing our results further, we outline the theoretical expectations for $\hat{q}$ and its relationship to η/s. To account for the temperature dependence of the coefficients η and $\hat{q}$, it is common practice to examine their dimensionless

counterparts: η/s, and $\hat{q}/T^3$ [102]. Both quantities are sensitive to the effective coupling strength in QGP. If the coupling is weak, η/s is large, while $\hat{q}/T^3$ is small. Conversely, when the coupling is strong, η/s becomes small, while $\hat{q}/T^3$ is large. In the case of weak coupling, it has been argued that these two quantities are related by $\frac{\eta}{s} \frac{\hat{q}}{T^3} \approx$ const, i.e., more specifically [40,102],

$$\frac{\eta}{s} \approx 1.25 \frac{T^3}{\hat{q}}. \qquad (16)$$

Furthermore, to explain the large observed high-$p_\perp$ v_2, it was proposed in Ref. [104], that the jet-quenching factor $\hat{q}/T^3$ must rise rapidly when approaching T_c from above. We *schematically* depicted such behavior in Fig. 7(a). This behavior is neither straightforward nor trivial to obtain from a model calculation.

The expected (qualitative) relation of the $T^3/\hat{q}$ and $(\eta/s)(T)$—based on the existing knowledge from previous
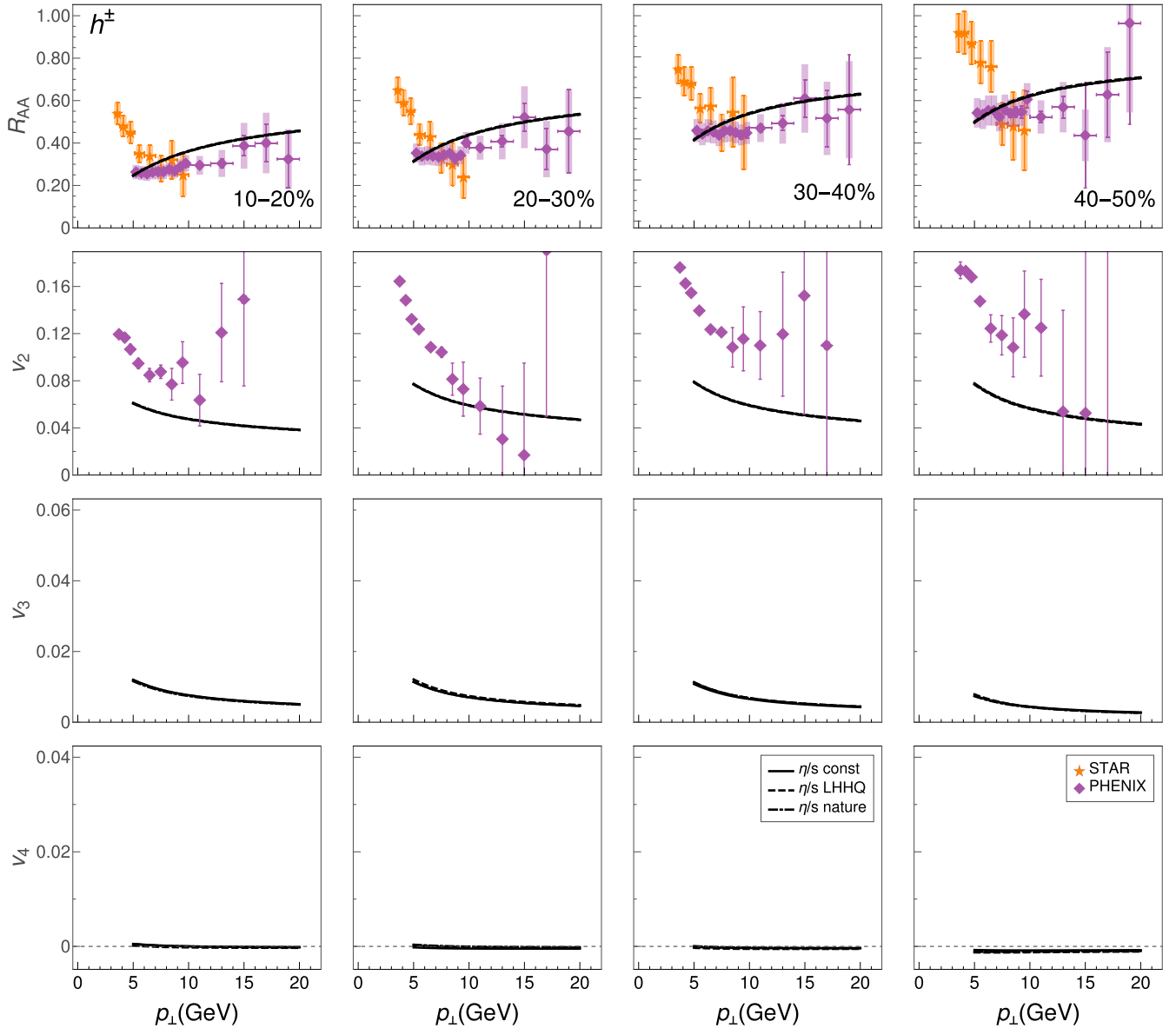
FIG. 4. The calculated charged hadron R_{AA} (first row), high-$p_\perp$ v_2 (second row), v_3 (third row), and v_4 (fourth row) in $\sqrt{s_{NN}} = 200$ GeV Au + Au collisions. The experimental data from the STAR (orange stars) [90] and PHENIX (purple diamonds) [91,92] Collaborations are also shown. Columns 1–4 represent the centrality classes 10–20%, 20–30%, 30–40%, and 40–50%, respectively.

studies—is *schematically* depicted in Fig. 7(b) [40]. At large temperatures, we expect the system to be weakly coupled. At that limit, our dynamical energy loss model should be applicable, and Eq. (16) should be a good approximation. Thus, we expect the calculated $T^3/\hat{q}$ to agree well with the inferred η/s as shown in the grey area at the right part of Fig. 7(b). On the other hand, in the strongly coupled limit [the left gray area in Fig. 7(b)] close to T_c, the calculated $T^3/\hat{q}$ is expected to significantly deviate from the inferred η/s. Interestingly, the $T^3/\hat{q}$ calculated using weak coupling methods is expected to drop below the inferred η/s [40], which, as known, is very close to the AdS-CFT lower limit of $1/(4\pi)$ in the vicinity of T_c.

The region between strongly and weakly coupled limits is the so-called "soft-to-hard" boundary [105], i.e., the region

where the transition from a strongly to a weakly coupled regime could take place. Therefore, plotting together η/s and $T^3/\hat{q}$ as a function of T might allow estimating the "soft-to-hard" boundary as the region where these two curves start to deviate, as schematically shown in Fig. 7(b).

We calculate $\hat{q}/T^3$ from our dynamical energy loss using Eq. (14) in the initial jet energy range $3 < E < 10$ GeV, as $p_\perp$ has to be low enough to mimic interactions of partons within the medium. The obtained result is shown in Fig. 8(a), and qualitatively similar to the expectation shown in Fig. 7(a). In particular, near T_c, we obtain an enhanced quenching, which is considerably larger than quenching in other energy loss models [76] (with the exception of [101], which got a substantial increase in $\hat{q}/T^3$ near T_c, due to a very large coupling in their model). Some models even
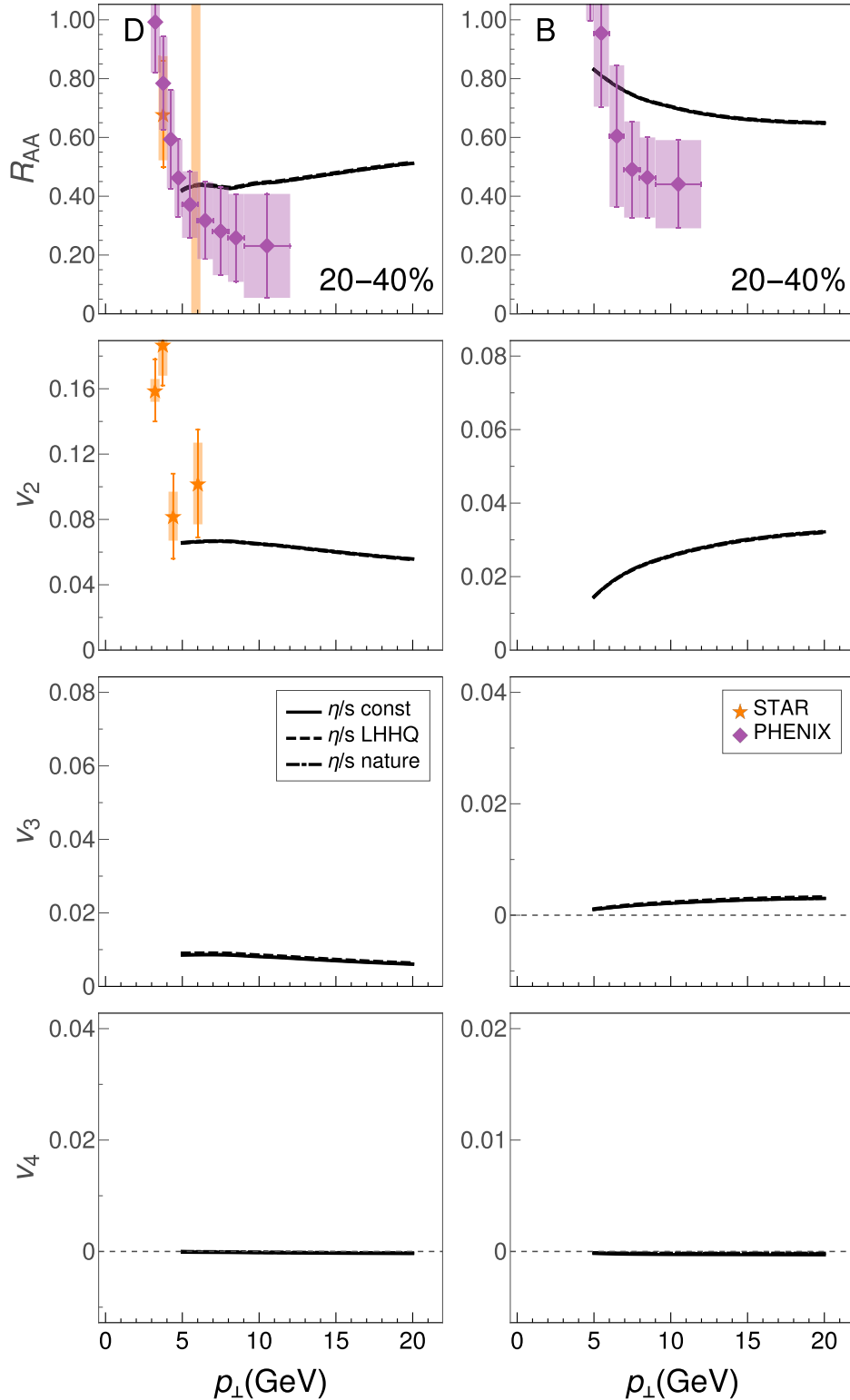
FIG. 5. D (left panel) and B meson (right panel) R_{AA} (first row) and high-$p_{\perp}$ flow harmonics v_2 (second row), v_3 (third row), and v_4 (fourth row) in $\sqrt{s_{NN}} = 200$ GeV Au + Au collisions in 20–40% centrality class. Theoretical predictions for D meson are compared with STAR (orange stars) [95] and preliminary PHENIX (purple diamonds) [96] data, whereas B meson predictions are compared with the preliminary PHENIX (purple diamonds) [96] data.
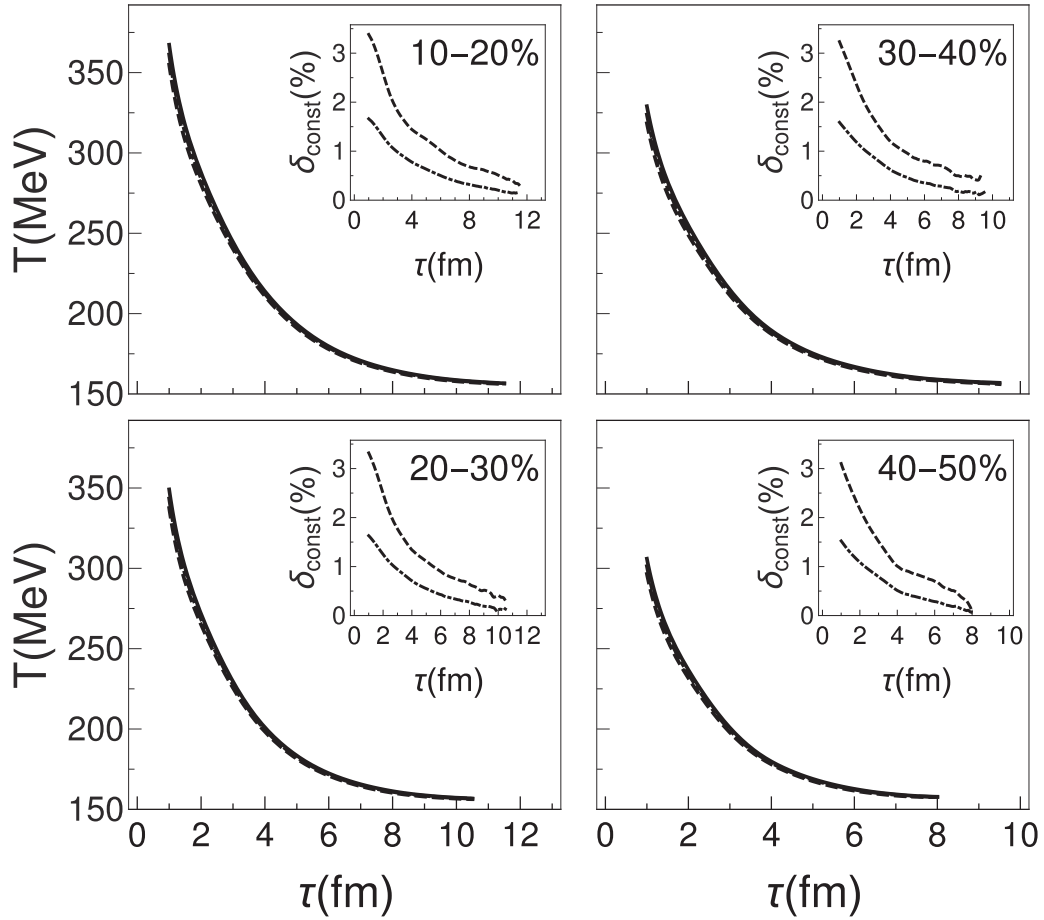
FIG. 6. The average temperature experienced by the jets as a function of proper time for three different $(\eta/s)(T)$ parametrizations in $\sqrt{s_{NN}} = 5.02$ TeV Pb + Pb collisions for four different centrality regions (10–20%, 20–30%, 30–40%, and 40–50%, as indicated in each panel). The inset shows the relative difference in jet-perceived temperature in case of "Nature" (dot-dashed curve) and "LHHQ" (dashed curve) with respect to constant η/s parametrizations.
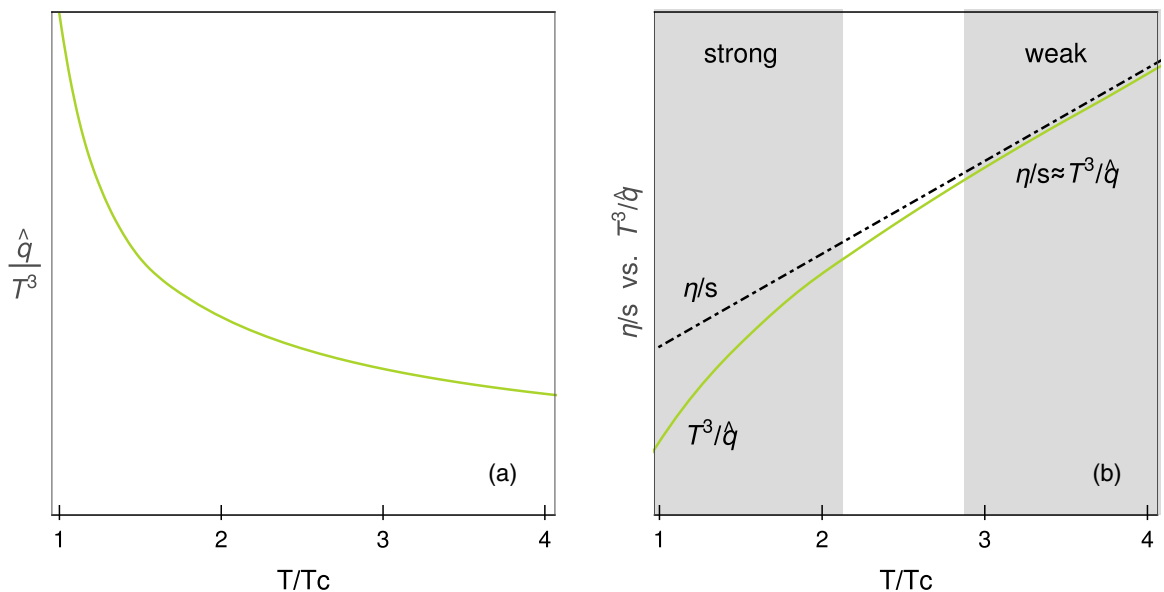

FIG. 7. (a) A schematic T dependence of quenching strength $\hat{q}/T^3$ proposed in [104]. (b) A scheme for mapping soft-to-hard boundary based on Ref. [40].
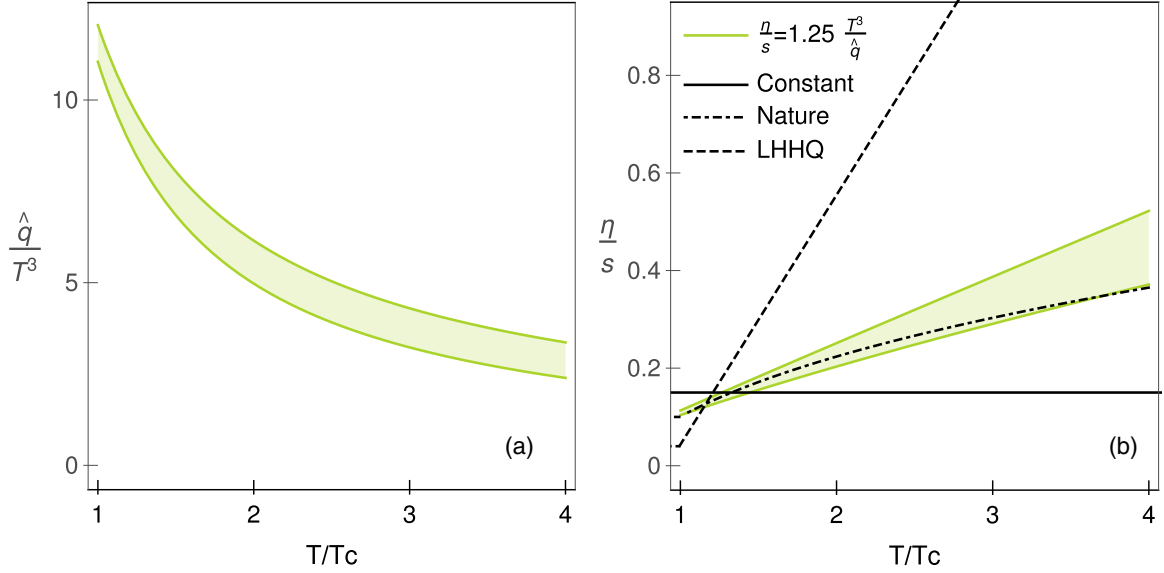
FIG. 8. (a) T dependence of $\hat{q}/T^3$ extracted from dynamical energy loss for initial jet energy in the range $E = 3$ GeV (lower boundary) to $E = 10$ GeV (upper boundary) [76]. (b) Comparison of η/s extracted from $\hat{q}/T^3$ [shown in (a)], with three different choices of the specific shear viscosity considered in this study and indicated in the legend.

predicted a decrease of $\hat{q}/T^3$ (or increase in η/s) when the temperature is approaching T_c from above [76,106,107]. The enhancement near T_c, obtained in Fig. 8(a), is due to an interplay between chromoelectric and chromomagnetic screenings [60]. As the magnetic component is inherently related to the dynamical nature of the medium constituents, it cannot exist in widely used static models, making the evolving medium an important feature of the dynamical energy loss model.

We convert our calculated $\hat{q}/T^3$ to $(\eta/s)(T)$ using Eq. (16), and compare it to the parametrizations used in this study in Fig. 8(b). First, the uncertainty due to the relevant initial jet energy is way smaller than the range of our $(\eta/s)(T)$ parametrizations. Second, our result is surprisingly close to the parametrization inspired by the Bayesian analysis of Ref. [18], "Nature," and, third, unexpectedly, our result obtained using weak coupling approximation does not drop significantly below the inferred η/s values in the vicinity of T_c.

To further gauge the significance of our result, we compare it to the 90% credible intervals for $(\eta/s)(T)$ obtained in two state-of-the-art Bayesian analyses [18,19] in Fig. 9. Interestingly, the η/s dependence extracted from our $\hat{q}/T^3$ shows an excellent agreement with both of these analyses in the entire T range, i.e., it falls precisely in the overlap of the two intervals. Our result agrees not only at large temperatures, where the Bayesian constraints are weakest, but even in the vicinity of T_c, where we expected our result to drop below the inferred values of η/s [as depicted in Fig. 7(b)]. This is a surprising result, as one might expect that our calculation of $\hat{q}$ from the dynamical energy loss model and Eq. (16) are reliable only in the weakly coupled regime. However, the agreement extends to T_c, i.e., to the regime corresponding to strong coupling.

While the extended agreement observed in Fig. 9 is encouraging in terms of the prediction ability of the dynamical

energy loss formalism, it leads to the question of why the expected behavior [shown schematically in Fig. 7(b)] is not observed in Fig. 9. It is unlikely that the weak coupling regime would extend down to T_c. Instead, it was suggested [40] that Eq. (16) is valid as long as the quasiparticle picture of QGP is applicable. The same is required for the validity of energy loss calculations, including our dynamical energy loss model. Therefore, it is an intriguing (and potentially significant)
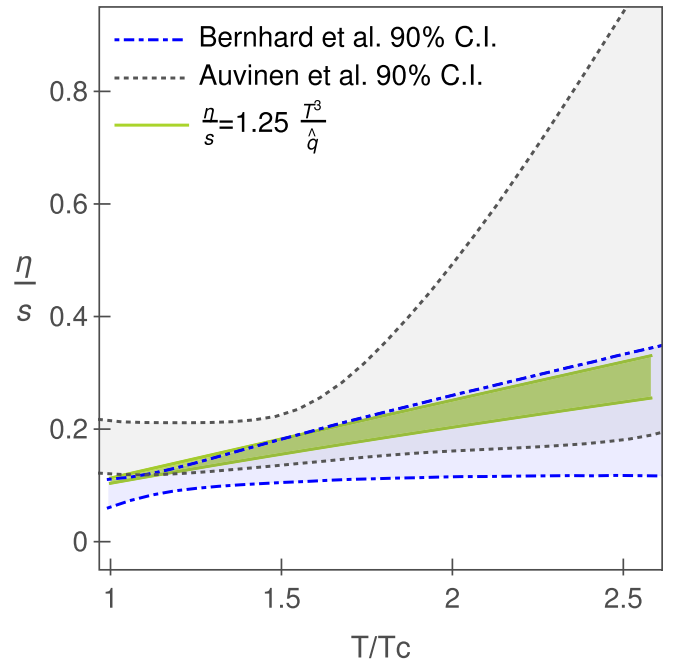

FIG. 9. Comparison of η/s extracted from $\hat{q}/T^3$ to the 90% credible intervals of the Bayesian analyses of Refs. [18,19] (Bernhard *et al.* and Auvinen *et al.*, respectively).

hypothesis that the quasiparticle picture used for describing interactions between jet and QGP is consistent with the QCD medium created at RHIC and LHC at the entire temperature range. In practical terms, this hypothesis is consistent with the dynamical energy loss model's ability to explain a wide range of experimental data.

Lastly, one of the open issues of QGP physics is mapping the "soft-to-hard" boundary. As discussed, a possible approach for estimating the boundary is to compare estimates of the same quantity (like η/s) from the high-$p_\perp$ and low-$p_\perp$ sectors, as schematically presented in Fig. 7(b). However, as shown here, the η/s obtained from high-$p_\perp$ theory and inferred from the low-$p_\perp$ data agree in the entire T range, providing no guidance on locating the boundary.

IV. SUMMARY

Our previous studies showed that combining high-$p_\perp$ predictions/data with temperature profiles from bulk medium simulations can constrain QGP medium properties, such as its early evolution and medium averaged anisotropy. Here we used an equivalent approach, where temperature profiles corresponding to different $(\eta/s)(T)$ parametrizations were generated and subsequently used by our generalized DREENA-A framework to generate predictions for R_{AA} and high-$p_\perp$ v_2, v_3, and v_4. However, we found that this approach cannot differentiate between temperature profiles generated using different $(\eta/s)(T)$ parametrizations, since the differences in T profiles and jet-perceived anisotropies [23] turned out to be small, and consequently the differences in high-$p_\perp$ predictions were also small. It is unrealistic to expect that the experiments at RHIC and LHC will (in a reasonable time frame) achieve the precision needed to distinguish between these predictions.

On the other hand, our second approach, based on calculating the quenching strength $\hat{q}/T^3$ from our dynamical energy loss model, showed a surprisingly good agreement with the constraints to $(\eta/s)(T)$ extracted from low-$p_\perp$ data by state-of-the-art Bayesian analysis. Such agreement is highly nontrivial as it originates from two entirely different approaches: A theoretical calculation based on finite temperature field theory through generalized HTL approach (dynamical energy loss) and inferring $(\eta/s)(T)$ from experimental data using fluid-dynamical modeling and advanced statistical (Bayesian) methods. The agreement is also surprising, as it extends all the way to T_c, where a strongly coupled regime should apply, and where a disagreement between energy loss calculation based on weak coupling approximation and inferred value of η/s is expected. We interpret the absence of such a disagreement in terms of the quasiparticle picture being valid even close to T_c. However, this obscures estimating soft-to-hard boundary, whose inference remains one of the field's major (to our knowledge, unresolved) problems. Overall, this work further emphasizes the utility of jet tomography, where low- and high-$p_\perp$ theory and data are jointly used to constrain the QGP properties.

[1] J. C. Collins and M. J. Perry, Phys. Rev. Lett. **34**, 1353 (1975).

[2] G. Baym and S. A. Chin, Phys. Lett. B **62**, 241 (1976).

[3] E. V. Shuryak, Phys. Lett. B **78**, 150 (1978).

[4] R. Stock, Nature (London) **337**, 319 (1989).

[5] M. Gyulassy and L. McLerran, Nucl. Phys. A **750**, 30 (2005).

[6] B. Jacak and P. Steinberg, Phys. Today **63**(5), 39 (2010).

[7] J. Stachel, Int. J. Mod. Phys. A **21**, 1750 (2006).

[8] P. F. Kolb and U. Heinz, in *Quark-Gluon Plasma 3*, edited by R. C. Hwa and X. N. Wang (World Scientific, Singapore, 2004).

[9] P. Romatschke and U. Romatschke, Phys. Rev. Lett. **99**, 172301 (2007).

[10] U. Heinz and R. Snellings, Annu. Rev. Nucl. Part. Sci. **63**, 123 (2013).

[11] J. Adams *et al.* (STAR Collaboration), Nucl. Phys. A **757**, 102 (2005).

[12] K. Adcox *et al.* (PHENIX Collaboration), Nucl. Phys. A **757**, 184 (2005).

[13] G. Aad *et al.* (ATLAS Collaboration), Phys. Rev. Lett. **105**, 252303 (2010).

[14] K. Aamodt *et al.* (ALICE Collaboration), Phys. Lett. B **696**, 30 (2011).

[15] J. Novak, K. Novak, S. Pratt, J. Vredevoogd, C. Coleman-Smith, and R. Wolpert, Phys. Rev. C **89**, 034917 (2014).

[16] S. Pratt, E. Sangaline, P. Sorensen, and H. Wang, Phys. Rev. Lett. **114**, 202301 (2015).

[17] J. E. Bernhard, arXiv:1804.06469.

[18] J. E. Bernhard, J. S. Moreland, and S. A. Bass, Nat. Phys. **15**, 1113 (2019).

[19] J. Auvinen, K. J. Eskola, P. Huovinen, H. Niemi, R. Paatelainen, and P. Petreczky, Phys. Rev. C **102**, 044911 (2020).

[20] D. Everett *et al.* (JETSCAPE Collaboration), Phys. Rev. C **103**, 054904 (2021).

[21] D. Everett *et al.* (JETSCAPE Collaboration), Phys. Rev. Lett. **126**, 242301 (2021).

[22] S. Stojku, J. Auvinen, M. Djordjevic, P. Huovinen, and M. Djordjevic, Phys. Rev. C **105**, L021901 (2022).

[23] S. Stojku, J. Auvinen, L. Zivkovic, P. Huovinen, and M. Djordjevic, Phys. Lett. B **835**, 137501 (2022).

[24] O. Soloveva, J. Aichelin, and E. Bratkovskaya, Phys. Rev. D **105**, 054011 (2022).

[25] W. J. Xing, S. Cao, and G. Y. Qin, arXiv:2303.12485.

[26] C. V. Johnson and P. Steinberg, Phys. Today **63**(5), 29 (2010).

[27] P. Kovtun, D. T. Son, and A. Starinets, Phys. Rev. Lett. **94**, 111601 (2005).

[28] U. Heinz *et al.*, arXiv:1501.06477.

[29] J. L. Nagle, I. G. Bearden, and W. A. Zajc, New J. Phys. **13**, 075004 (2011).

[30] H. Niemi, G. S. Denicol, P. Huovinen, E. Molnar, and D. H. Rischke, Phys. Rev. Lett. **106**, 212302 (2011).

[31] H. Niemi, G. S. Denicol, P. Huovinen, E. Molnar, and D. H. Rischke, Phys. Rev. C **86**, 014909 (2012).

[32] G. Nijs and W. van der Schee, Phys. Rev. Lett. **129**, 232301 (2022).

[33] M. R. Heffernan, C. Gale, S. Jeon, and J. F. Paquet, arXiv:2302.09478.

[34] D. Zigic, J. Auvinen, I. Salom, M. Djordjevic, and P. Huovinen, Phys. Rev. C **106**, 044909 (2022).

[35] D. Zigic, I. Salom, J. Auvinen, P. Huovinen, and M. Djordjevic, Front. Phys. **10**, 957019 (2022).

[36] M. Djordjevic, Phys. Rev. C **74**, 064907 (2006).

[37] M. Djordjevic, Phys. Rev. C **80**, 064909 (2009).

[38] M. Djordjevic and U. W. Heinz, Phys. Rev. Lett. **101**, 022302 (2008).

[39] T. Renk, Phys. Rev. C **85**, 044903 (2012).

[40] A. Majumder, B. Müller, and X.-N. Wang, Phys. Rev. Lett. **99**, 192301 (2007).

[41] H. Song and U. W. Heinz, Phys. Rev. C **77**, 064901 (2008).

[42] H. Song and U. W. Heinz, Phys. Rev. C **78**, 024902 (2008).

[43] J. E. Bernhard, J. S. Moreland, S. A. Bass, J. Liu, and U. Heinz, Phys. Rev. C **94**, 024907 (2016).

[44] https://github.com/Duke-QCD/hic-eventgen.

[45] W. Israel and J. M. Stewart, Ann. Phys. **118**, 341 (1979).

[46] A. Bazavov *et al.* (HotQCD Collaboration), Phys. Rev. D **90**, 094503 (2014).

[47] F. Cooper and G. Frye, Phys. Rev. D **10**, 186 (1974).

[48] S. A. Bass *et al.*, Prog. Part. Nucl. Phys. **41**, 255 (1998).

[49] M. Bleicher *et al.*, J. Phys. G **25**, 1859 (1999).

[50] J. S. Moreland, J. E. Bernhard, and S. A. Bass, Phys. Rev. C **92**, 011901 (2015).

[51] M. Djordjevic and M. Djordjevic, Phys. Rev. C **92**, 024918 (2015).

[52] M. Djordjevic, S. Stojku, M. Djordjevic, and P. Huovinen, Phys. Rev. C **100**, 031901 (2019).

[53] S. Acharya *et al.* (ALICE Collaboration), Phys. Rev. C **101**, 044907 (2020).

[54] S. S. Adler *et al.* (PHENIX Collaboration), Phys. Rev. C **69**, 034909 (2004).

[55] J. Adam *et al.* (ALICE Collaboration), Phys. Rev. Lett. **116**, 132302 (2016).

[56] J. Adams *et al.* (STAR Collaboration), Phys. Rev. C **72**, 014904 (2005).

[57] J. I. Kapusta, *Finite Temperature Field Theory* (Cambridge University Press, Cambridge, 1989).

[58] B. Blagojevic, M. Djordjevic, and M. Djordjevic, Phys. Rev. C **99**, 024901 (2019).

[59] M. Djordjevic and M. Djordjevic, Phys. Lett. B **734**, 286 (2014).

[60] M. Djordjevic and M. Djordjevic, Phys. Lett. B **709**, 229 (2012).

[61] S. Stojku, B. Ilic, I. Salom, and M. Djordjevic, Phys. Rev. C **108**, 044905 (2023).

[62] S. Wicks, W. Horowitz, M. Djordjevic, and M. Gyulassy, Nucl. Phys. A **784**, 426 (2007).

[63] Z. B. Kang, I. Vitev, and H. Xing, Phys. Lett. B **718**, 482 (2012).

[64] R. Sharma, I. Vitev, and B. W. Zhang, Phys. Rev. C **80**, 054902 (2009).

[65] M. Cacciari, S. Frixione, N. Houdeau, M. L. Mangano, P. Nason, and G. Ridolfi, J. High Energy Phys. 10 (2012) 137.

[66] D. de Florian, R. Sassot, and M. Stratmann, Phys. Rev. D **75**, 114010 (2007).

[67] M. Cacciari and P. Nason, J. High Energy Phys. 09 (2003) 006.

[68] E. Braaten, K. Cheung, S. Fleming, and T. C. Yuan, Phys. Rev. D **51**, 4819 (1995).

[69] V. G. Kartvelishvili, A. K. Likhoded, and V. A. Petrov, Phys. Lett. B **78**, 615 (1978).

[70] A. Peshier, arXiv:hep-ph/0601119.

[71] S. Cao and X. N. Wang, Rep. Prog. Phys. **84**, 024301 (2021).

[72] A. Nakamura, T. Saito, and S. Sakai, Phys. Rev. D **69**, 014506 (2004).

[73] M. Djordjevic and M. Gyulassy, Phys. Rev. C **68**, 034914 (2003).

[74] S. Borsányi, Z. Fodor, S. D. Katz, A. Pásztor, K. K. Szabó, and C. Török, J. High Energy Phys. 04 (2015) 138.

[75] R. Baier, Y. Dokshitzer, A. Mueller, S. Peigne, and D. Schiff, Nucl. Phys. B **484**, 265 (1997).

[76] K. M. Burke *et al.* (JET Collaboration), Phys. Rev. C **90**, 014909 (2014).

[77] S. Peigne and A. Peshier, Phys. Rev. D **77**, 114017 (2008).

[78] R. Rapp *et al.*, Nucl. Phys. A **979**, 21 (2018).

[79] A. M. Sirunyan *et al.* (CMS Collaboration), Phys. Lett. B **776**, 195 (2018).

[80] V. Khachatryan *et al.* (CMS Collaboration), J. High Energy Phys. 04 (2017) 039.

[81] S. Acharya *et al.* (ALICE Collaboration), J. High Energy Phys. 11 (2018) 013.

[82] S. Acharya *et al.* (ALICE Collaboration), J. High Energy Phys. 07 (2018) 103.

[83] M. Aaboud *et al.* (ATLAS), Eur. Phys. J. C **78**, 997 (2018).

[84] G. Aad *et al.* (ATLAS), J. High Energy Phys. 07 (2023) 074.

[85] A. M. Sirunyan *et al.* (CMS Collaboration), Phys. Lett. B **816**, 136253 (2021).

[86] S. Acharya *et al.* (ALICE Collaboration), J. High Energy Phys. 01 (2022) 174.

[87] S. Acharya *et al.* (ALICE Collaboration), Phys. Lett. B **813**, 136054 (2021).

[88] Contribution link: https://indico.cern.ch/event/895086/contributions/4314625/.

[89] Contribution link: https://indico.cern.ch/event/895086/contributions/4715758/.

[90] J. Adams *et al.* (STAR Collaboration), Phys. Rev. Lett. **91**, 172302 (2003).

[91] A. Adare *et al.* (PHENIX Collaboration), Phys. Rev. C **87**, 034911 (2013).

[92] A. Adare *et al.* (PHENIX Collaboration), Phys. Rev. C **99**, 054903 (2019).

[93] M. Djordjevic, M. Djordjevic, and B. Blagojevic, Phys. Lett. B **737**, 298 (2014).

[94] D. Zigic, I. Salom, J. Auvinen, M. Djordjevic, and M. Djordjevic, J. Phys. G **46**, 085101 (2019).

[95] L. Adamczyk *et al.* (STAR Collaboration), Phys. Rev. Lett. **113**, 142301 (2014); **121**, 229901(E) (2018).

[96] Contribution link: https://indico.cern.ch/event/895086/contributions/4744010/.

[97] X. Guo and X.-N. Wang, Phys. Rev. Lett. **85**, 3591 (2000).

[98] A. Majumder, Phys. Rev. D **85**, 014023 (2012).

[99] J. Barata, Y. Mehtar-Tani, A. Soto-Ontoso, and K. Tywoniuk, Phys. Rev. D **104**, 054047 (2021).

[100] C. Sirimanna, S. Cao, and A. Majumder, Phys. Rev. C **105**, 024908 (2022).

[101] I. Grishmanovskii, T. Song, O. Soloveva, C. Greiner, and E. Bratkovskaya, Phys. Rev. C **106**, 014903 (2022).

[102] B. Müller, Phys. Rev. D **104**, L071501 (2021).

[103] J. Wu, S. Cao, and F. Li, arXiv:2208.14297.

[104] J. Liao and E. Shuryak, Phys. Rev. Lett. **102**, 202302 (2009).

[105] B. Betz and M. Gyulassy, Nucl. Phys. A **931**, 410 (2014).

[106] A. Majumder and M. Van Leeuwen, Prog. Part. Nucl. Phys. **66**, 41 (2011).

[107] R. Marty, E. Bratkovskaya, W. Cassing, J. Aichelin, and H. Berrehrah, Phys. Rev. C **88**, 045204 (2013).